

# Shock–turbulence interaction in core-collapse supernovae

Ernazar Abdikamalov,<sup>1</sup>★ Azamat Zhaksylykov,<sup>1</sup> David Radice<sup>2</sup>  
and Shapagat Berdibek<sup>1</sup>

<sup>1</sup>Department of Physics, School of Science and Technology, Nazarbayev University, Astana 010000, Kazakhstan

<sup>2</sup>TAPIR, MC 350-17, California Institute of Technology, 1200 E California Blvd., Pasadena, CA 91125, USA

Accepted 2016 July 1. Received 2016 July 1; in original form 2016 May 29

## ABSTRACT

Nuclear shell burning in the final stages of the lives of massive stars is accompanied by strong turbulent convection. The resulting fluctuations aid supernova explosion by amplifying the non-radial flow in the post-shock region. In this work, we investigate the physical mechanism behind this amplification using a linear perturbation theory. We model the shock wave as a one-dimensional planar discontinuity and consider its interaction with vorticity and entropy perturbations in the upstream flow. We find that, as the perturbations cross the shock, their total turbulent kinetic energy is amplified by a factor of  $\sim 2$ , while the average linear size of turbulent eddies decreases by about the same factor. These values are not sensitive to the parameters of the upstream turbulence and the nuclear dissociation efficiency at the shock. Finally, we discuss the implication of our results for the supernova explosion mechanism. We show that the upstream perturbations can decrease the critical neutrino luminosity for producing explosion by several per cent.

**Key words:** hydrodynamics – shock waves – turbulence – supernovae: general.

## 1 INTRODUCTION

Massive stars undergo vigorous convective shell burning at the end of their lives (e.g. Arnett, Meakin & Young 2009; Takahashi & Yamada 2014; Couch et al. 2015; Chatzopoulos et al. 2016; Müller et al. 2016). The associated non-radial dynamics and the deviations from spherical symmetry can grow further during collapse (Lai & Goldreich 2000; Takahashi & Yamada 2014). Recent works by Couch & Ott (2013, 2015) and Müller & Janka (2015) demonstrate that such asphericities facilitate supernova explosion. According to Couch & Ott (2015) and Müller & Janka (2015), this is a result of increased turbulent activity in the post-shock region driven by the passage of the upstream fluctuations through the shock. The non-radial dynamics in the post-shock region is an important factor that aids the expansion of the supernova shock (e.g. Burrows, Hayes & Fryxell 1995; Herant 1995; Janka & Müller 1996; Blondin, Mezzacappa & DeMarino 2003; Foglizzo, Scheck & Janka 2006; Foglizzo et al. 2007, 2015; Hanke et al. 2012, 2013; Janka et al. 2012; Burrows 2013; Dolence et al. 2013; Murphy, Dolence & Burrows 2013; Ott et al. 2013; Takiwaki, Kotake & Suwa 2014; Abdikamalov et al. 2015; Cardall & Budiardja 2015; Fernández 2015; Lentz et al. 2015; Melson, Janka & Marek 2015a; Melson et al. 2015b; Radice, Couch & Ott 2015; Bruenn et al. 2016; Janka, Melson & Summa 2016; Radice et al. 2016; Roberts et al. 2016).

In this work, we investigate the physics of the interaction of the upstream turbulence with the supernova shock and its effect on the post-shock flow using a linear perturbation theory commonly known as the linear interaction approximation (LIA) theory. The LIA, which we extend to include the nuclear dissociation at the shock, is a powerful tool originally developed in the 1950s by Ribner (1953), Moore (1954), and Chang (1957), followed by other works (e.g. Ribner 1954; Chang 1957; McKenzie & Westphal 1968; Jackson, Kapila & Hussaini 1990; Mahesh, Moin & Lele 1996; Duck, Lasseigne & Hussaini 1997; Mahesh, Lele & Moin 1997; Fabre, Jacquin & Sesterhenn 2001; Wouchuk, Huete Ruiz de Lira & Velikovich 2009; Huete Ruiz de Lira, Velikovich & Wouchuk 2011; Huete, Wouchuk & Velikovich 2012; Huete, Sánchez & Williams 2013, 2014).

In the LIA, the shock is modelled as a planar discontinuity with no intrinsic scale and the flow is decomposed into the mean and fluctuating parts. Both components can be specified arbitrarily in the upstream flow. Once the upstream field is specified, the downstream field can be fully determined using the Rankine–Hugoniot jump conditions at the shock (e.g. Sagaut & Cambon 2008). The LIA is valid in the regime of sufficiently small fluctuations such that the mean flow satisfies the usual jump conditions, while the turbulent fluctuations satisfy the linearized jump conditions. Numerical simulations by Lee, Lele & Moin (1993) suggest that this approximation is valid when

$$\mathcal{M}^2 \lesssim 0.1(\mathcal{M}_1^2 - 1), \quad (1)$$

★ E-mail: ernazar.abdikamalov@nu.edu.kz

where  $\mathcal{M}'$  and  $\mathcal{M}_1$  are the Mach number of upstream turbulence and mean flow, respectively (see also Ryu & Livescu 2014). In massive star shell convection,  $\mathcal{M}' \sim 0.1$  (e.g. Müller et al. 2016), which at most can increase by a factor of several during contraction (more precise calculation of this is given in Section 4). Since  $\mathcal{M}_1 \gtrsim 5$  in core-collapse supernovae (CCSNe), condition (1) is well satisfied and we expect the LIA to be an excellent approximation for studying the interaction of CCSN shocks with progenitor asphericities.

## 2 THE LINEAR INTERACTION APPROXIMATION

The LIA employs the Kovasznay (1953) decomposition of the fluctuating field, according to which any small fluctuations in a turbulent flow can be decomposed into individual Fourier modes that are characterized by their type, wavenumber, and frequency. There are three types of modes: vorticity, entropy, and acoustic modes. The vorticity mode is a solenoidal velocity field that is advected with the mean flow. It has no pressure or density fluctuations. The entropy mode is also advected with the flow and it represents density and temperature fluctuations with no associated pressure or velocity variations. The acoustic mode represents sound waves that travel relative to the mean flow. It has isentropic pressure and density fluctuations and irrotational velocity field. All Kovasznay modes evolve independently in the limit of weak fluctuations and the interaction of each mode with the shock wave can be studied independently. Integration over all individual modes yields the full statistics of the turbulent flow (e.g. Sagaut & Cambon 2008).

We assume that the shock wave is a planar discontinuity and we choose our  $x$ -axis ( $y$ -axis) to be perpendicular (parallel) to the shock front. The average shock position is assumed to be at  $x = 0$  and the mean flow is in the positive  $x$  direction. The quantities  $U$ ,  $\bar{\rho}$ ,  $\bar{p}$ ,  $\bar{T}$ , and  $\mathcal{M}$  represent the mean velocity, density, pressure, temperature, and Mach number. We choose the values of these parameters to approximate the CCSN shock by requiring vanishing Bernoulli parameter for the upstream flow, as described in Appendix A. We employ a gamma-law equation of state with  $\gamma = 4/3$ . The quantities  $u'$ ,  $v'$ ,  $\rho'$ ,  $p'$ , and  $T'$  denote the perturbation in the  $x$ - and  $y$ -components of velocity, density, pressure, and temperature, respectively. Hereafter, subscripts 1 and 2 will denote the upstream and downstream states. The upstream vorticity mode is modelled via a planar shear wave with wavenumber  $(m\kappa, l\kappa)$  and angular frequency  $\kappa m U_1$ :

$$\frac{u'_1}{U_1} = l A_v e^{i\kappa(mx+ly-U_1mt)}, \quad (2)$$

$$\frac{v'_1}{U_1} = -m A_v e^{i\kappa(mx+ly-U_1mt)}, \quad (3)$$

while the upstream entropy mode is given by another planar sinusoidal wave with the same wavenumber and frequency,

$$\frac{\rho'_1}{\bar{\rho}_1} = A_e e^{i\kappa(mx+ly-U_1mt)}, \quad (4)$$

$$\frac{T'_1}{\bar{T}_1} = -\frac{\rho'_1}{\bar{\rho}_1}, \quad (5)$$

where  $m = \cos \psi_1$  and  $l = \sin \psi_1$  and  $\psi_1$  is the angle between the  $x$ -axis and the direction of propagation of the incident perturbation.  $A_v$  and  $A_e$  are the amplitudes of the incident vorticity and entropy waves, respectively. In the present work, we ignore acoustic waves in the pre-shock region, which corresponds to the assumption of zero pressure fluctuations in the upstream flow ( $p'_1 = 0$ ). The effect

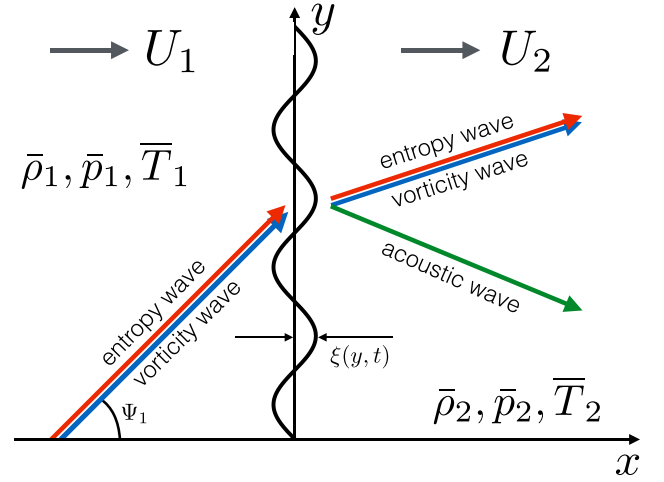


**Figure 1.** Schematic representation of the interaction of an entropy and/or vorticity waves with a shock wave in the context of the LIA formalism. The average position of the shock is aligned with the  $y$ -axis and the mean flow is in the positive  $x$  direction. The upstream mean flow is characterized by velocity  $U_1$ , density  $\bar{\rho}_1$ , pressure  $\bar{p}_1$ , and temperature  $\bar{T}_1$ , while the corresponding downstream quantities are  $U_2$ ,  $\bar{\rho}_2$ ,  $\bar{p}_2$ , and  $\bar{T}_2$ . When vorticity and/or entropy waves of form (2)–(5) hit a shock wave, the latter responds by changing its position and shape. In the framework of LIA, for such perturbations, the shock surface deforms into a sinusoidal planar wave propagating in the  $y$ -direction described by formula (6). The downstream perturbation field consists of entropy, vorticity, and acoustic waves given by equations (7)–(11).

of the upstream acoustic component will be studied in our future work.

When vorticity and/or entropy waves hit a shock wave, the latter responds by changing its position and shape. In the framework of the LIA, for a perturbation of form (2)–(5), the shock surface deforms into a shape of a sinusoidal wave propagating in the  $y$ -direction:

$$\xi(y, t) = -\frac{L}{i\kappa m} e^{i\kappa(l y - U_1 m t)}, \quad (6)$$

where  $\xi(y, t)$  is the  $x$ -coordinate of the shock position at time  $t$  and ordinate  $y$  and  $L$  is a quantity that characterizes the amplitude of the shock oscillations (cf. Fig. 1).

The interaction of the vorticity and entropy waves with the shock generates a downstream perturbation field consisting of vorticity, entropy, and acoustic waves given by (Mahesh et al. 1996, 1997)

$$\frac{u'_2}{U_1} = F e^{i\kappa x} e^{i\kappa(l y - U_1 m t)} + G e^{i\kappa(C m x + l y - U_1 m t)}, \quad (7)$$

$$\frac{v'_2}{U_1} = H e^{i\kappa x} e^{i\kappa(l y - U_1 m t)} + I e^{i\kappa(C m x + l y - U_1 m t)}, \quad (8)$$

$$\frac{p'_2}{\bar{p}_2} = K e^{i\kappa x} e^{i\kappa(l y - U_1 m t)}, \quad (9)$$

$$\frac{\rho'_2}{\bar{\rho}_1} = \frac{K}{\gamma} e^{i\kappa x} e^{i\kappa(l y - U_1 m t)} + Q e^{i\kappa(C m x + l y - U_1 m t)}, \quad (10)$$

$$\frac{T'_2}{\bar{T}_1} = \frac{(\gamma - 1)K}{\gamma} e^{i\kappa x} e^{i\kappa(l y - U_1 m t)} - Q e^{i\kappa(C m x + l y - U_1 m t)}. \quad (11)$$

The schematic representation of this process is depicted in Fig. 1. Note that these waves have the same angular frequencies and  $y$ -components of wavenumbers as those of the upstream waves

(2)–(5). The coefficients  $F$ ,  $H$ , and  $K$  are the amplitudes of the acoustic component, while coefficients  $G$ ,  $I$ , and  $Q$  are associated with the entropy and vorticity components. The latter two components have the same wavenumber vector ( $mC\kappa, l\kappa$ ) and angular frequency  $\kappa mU_1$ , for which reason they are often referred to as entropy–vorticity waves. The acoustic component has the same angular frequency but different wavenumber ( $\tilde{\kappa}, l\kappa$ ), where  $\tilde{\kappa}$  is calculated in Appendix B. The parameter  $C$  is the compression factor at the shock,  $C = \bar{\rho}_2/\bar{\rho}_1 = U_1/U_2$ , which can be obtained from the Rankine–Hugoniot condition as (cf. Appendix A)

$$C = \frac{\gamma + 1}{\gamma + \frac{1}{M_1^2} - \sqrt{\left(1 - \frac{1}{M_1^2}\right)^2 + (\gamma + 1)\frac{(\gamma-1)M_1^2+2}{M_1^2}\bar{\epsilon}}}. \quad (12)$$

Here,  $\bar{\epsilon}$  is the dimensionless nuclear dissociation parameter, which characterizes nuclear dissociation energy, as explained in Appendix A. It typically ranges from 0, which represents the limit corresponding to zero nuclear dissociation, to 0.4, which represents strong nuclear dissociation. We adopt  $\bar{\epsilon} = 0.2$  and  $M_1 = 5$  as our fiducial values.

In order to obtain the coefficients  $F$ ,  $G$ ,  $H$ ,  $I$ ,  $K$ ,  $Q$ ,  $L$ , we first expand the Rankine–Hugoniot conditions to the first order in amplitudes of incoming perturbations (Ribner 1953; Chang 1957; Mahesh et al. 1997). The solution of the resulting equations yields the coefficients  $F$ ,  $G$ ,  $H$ ,  $I$ ,  $K$ ,  $Q$ ,  $L$ , as we demonstrate in Appendix B.

The downstream acoustic component depends strongly on the incidence angle  $\psi_1$ . If  $\psi_1$  is smaller than the critical angle

$$\psi_c = \cot^{-1} \sqrt{\frac{c_{s,2}^2}{U_1^2} - \frac{U_2^2}{U_1^2}}, \quad (13)$$

where  $c_{s,2}$  is the downstream speed of sound, then  $\tilde{\kappa}$  is real and the sound waves represent freely propagating planar sine waves. On the other hand, if  $\psi_c < \psi_1$ ,  $\tilde{\kappa}$  is complex and the solution represents an exponentially damping planar sine wave (Mahesh et al. 1996, 1997).

A detailed derivation of the LIA equations, including angle  $\psi_c$  (13) and wavenumber  $\tilde{\kappa}$  in equations (7)–(11), is presented in Appendix B.

### 3 RESULTS

The key quantity affecting the evolution of the flow through a shock wave is the compression factor  $C$ . Fig. 2 shows  $C$  as a function of the nuclear dissociation parameter  $\bar{\epsilon}$  for four values of upstream Mach number  $M_1$ : 2.5, 5, 10, and 100. For all of these values, the compression factor  $C$  grows with increasing  $\bar{\epsilon}$ , meaning that the nuclear dissociation leads to stronger compression. Note that the values of the compression factor  $C$  are very close to each other for  $M_1 = 5$ , 10, and 100. This is a generic property of shock waves, in which the compression factor depends on  $M_1$  very weakly when  $M_1 \gtrsim 5$ .

In the following, we present our results in two parts. In the first part (Section 3.1), we discuss the interaction of a shock wave with individual incident waves and explore how it depends on shock and perturbation parameters. In the second part (Section 3.2), we investigate the interaction of a shock wave with incident turbulence fields, which we model as sets of random entropy and vorticity waves.

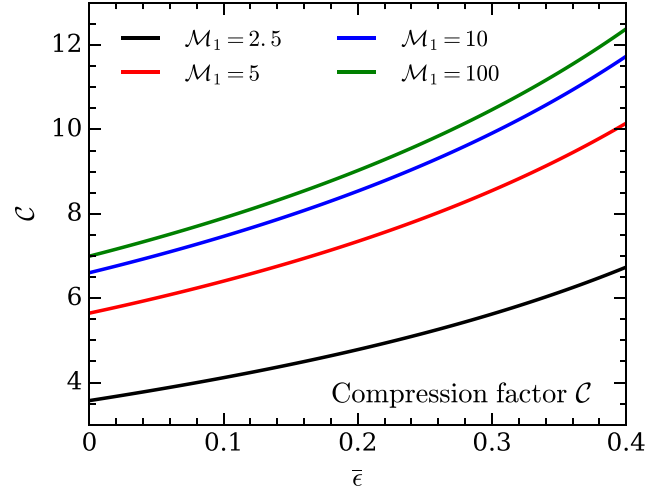


**Figure 2.** The compression factor  $C$  at the shock as a function of nuclear dissociation parameter  $\bar{\epsilon}$  for four values of upstream Mach number  $M_1$ : 2.5, 5, 10, and 100. In all of these cases, the compression factor  $C$  increases with  $\bar{\epsilon}$ , signifying that the nuclear dissociation leads to stronger compression.

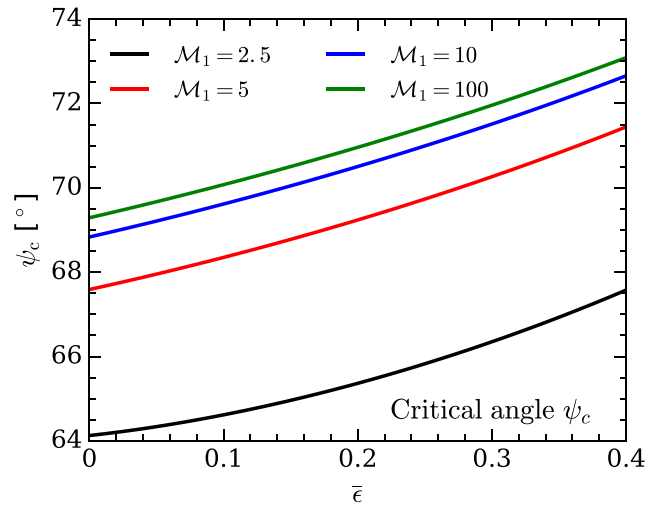


**Figure 3.** The critical angle  $\psi_c$  as a function of nuclear dissociation parameter  $\bar{\epsilon}$  for four values of upstream Mach number  $M_1$ : 2.5, 5, 10, and 100.

#### 3.1 Interaction with a single wave

Fig. 3 shows the values of the critical angle  $\psi_c$  as a function of nuclear dissociation parameter  $\bar{\epsilon}$  for four values of upstream Mach number  $M_1$ : 2.5, 5, 10, and 100. Recall that the critical angle  $\psi_c$  separates two regions of the solution: propagative ( $\psi_1 < \psi_c$ ) and non-propagative ( $\psi_1 > \psi_c$ ). The first is characterized by acoustic waves in the post-shock flow, while in the second sound waves do not propagate. In all cases,  $\psi_c$  increases with  $\bar{\epsilon}$ . However, this increase is rather modest. For example, for  $M_1 = 5$ ,  $\psi_c$  increases from 67.6 to only 71.5 as  $\bar{\epsilon}$  increases from 0 to 0.4. These values do not change much with  $M_1$  after  $M_1 = 5$ . This is a simple reflection of the above-mentioned fact that the compression factor does not depend strongly on the upstream Mach number for  $M_1 \gtrsim 5$ .

For an incident vorticity wave of form given by equations (2) and (3), the velocity field is  $u'_1 \propto \sin \psi_1$  and  $v'_1 \propto \cos \psi_1$ . If the perturbation wavenumber vector  $\mathbf{k}$  is perpendicular to the shock

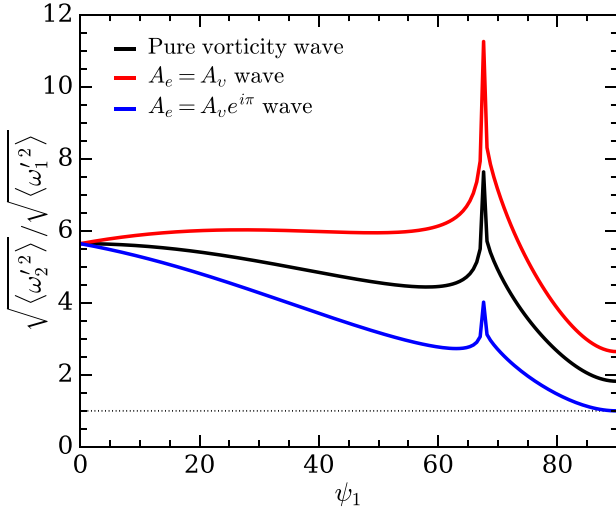


**Figure 4.** The amplification of vorticity across the shock as a function of angle  $\psi$  for incident vorticity wave, in-phase vorticity–entropy wave (i.e.  $A_e = A_v$ ), and out-of-phase vorticity–entropy wave (i.e.  $A_e = A_v e^{i\pi}$ ). The upstream Mach number is  $\mathcal{M}_1 = 5$ . When the vorticity and entropy waves are in phase, we get strongest amplification. When they are out of phase, we get the weakest amplification. The horizontal dotted black line with  $y = 1$  is added as a reference line for a better readability of the plots.

wave ( $\psi_1 = 0$ ), the  $x$ -component of the fluctuation field is zero. When such a field hits the shock, the solution is trivial: the shock wave is not affected and the velocity passes through the shock without any modifications, i.e.  $v_2' = v_1'$  and  $u_2' = u_1' = 0$ . The only property that changes is the  $x$ -component of the wavenumber: it increases by a factor of  $\mathcal{C}$ . Correspondingly, the wavelength of the wave decreases by the same factor.

The situation is drastically different when  $\psi_1 > 0$ . The perturbation velocity field now has non-zero  $x$ -component, which forces the shock surface to oscillate according to equation (6). Because of this, the downstream field now consists of not only vorticity waves, but also of entropy and acoustic waves, as described by equations (7)–(11). Both entropy and vorticity waves in the post-shock region have the same wavenumber vector ( $\mathcal{C}m\kappa, l\kappa$ ). Thus, the magnitude of the wavenumber vector increases by factor

$$\frac{\kappa_2}{\kappa_1} = \sqrt{\mathcal{C}^2 m^2 + l^2}, \quad (14)$$

as the wave crosses the shock. Accordingly, the wavelength of the mode decreases by the same factor across the shock.

Fig. 4 shows the ratio of averaged pre-shock and post-shock vorticities  $\sqrt{\langle \omega_2'^2 \rangle} / \sqrt{\langle \omega_1'^2 \rangle}$  as a function of angle  $\psi_1$  for  $\mathcal{M}_1 = 5$  and  $\bar{\epsilon} = 0$ .<sup>1</sup> Here, brackets  $\langle \rangle$  mean averaging over time  $t$  and the  $y$ -coordinate. The solid black line represents the case of incident vorticity wave. The case of incident entropy and vorticity waves of the same amplitude and phase (i.e.  $A_e = A_v$ ) is shown with red line, while the same with 180° phase difference (i.e.  $A_e = A_v e^{i\pi}$ )

<sup>1</sup> Note that since the flow is restricted to  $x$ – $y$  plane, vorticity has only the  $z$ -component:

$$\omega_1' = \partial_x v_1' - \partial_y u_1' = -ik A_v e^{ik(mx + ly - U_1 mt)}. \quad (15)$$

As we show below, this is not a restriction because a general three-dimensional (3D) problem can be expressed in terms of a two-dimensional (2D) LIA problem.

is represented by the blue line. As we can see, when the vorticity and entropy waves are in phase, we get a significantly stronger amplification. When they are out of phase, we get the weakest amplification. Finally, in the case of pure vorticity incident wave, the amplification is roughly the average of these two regimes. For example, for  $\psi_1 = 60^\circ$ , we get  $\sqrt{\langle \omega_2'^2 \rangle} / \sqrt{\langle \omega_1'^2 \rangle}$  of 6.14, 2.77, and 4.46 in these three cases. The spike in  $\sqrt{\langle \omega_2'^2 \rangle} / \sqrt{\langle \omega_1'^2 \rangle}$  around  $\psi_1 \simeq 69^\circ$  corresponds to the critical angle  $\psi_1 = \psi_c$ .

In order to explain the behaviour of the vorticity fluctuations  $\omega'$ , Mahesh et al. (1996, 1997) developed a simple model, which we present here for completeness. Linearizing the Euler equations about the mean flow and neglecting the incident pressure perturbations, we get the following equation for the vorticity fluctuations  $\omega'$  (Mahesh et al. 1996):

$$\omega_t' + U \omega_x' = -\omega' U_x - \frac{\rho_y'}{\bar{\rho}^2} \bar{p}_x, \quad (16)$$

where subscripts  $t$  and  $x$  mean partial derivatives with respect to these variables. The first term on the right-hand side of this equation ( $-\omega' U_x$ ) represents the effect of the bulk compression. Since velocity drops across the shock, it amplifies the vorticity. The second term ( $-\frac{\rho_y'}{\bar{\rho}^2} \bar{p}_x$ ) represents the baroclinic processes, which produce vorticity even from pure entropy perturbations. It can either amplify or weaken the effect of bulk compression depending on the relative phase between the vorticity and entropy waves. For incident vorticity and entropy waves of form (2)–(5), equation (16) reduces to

$$-\omega' U_x - \frac{\rho_y'}{\bar{\rho}^2} \bar{p}_x \sim A_v U U_x - A_e l \frac{p_x'}{\bar{\rho}}. \quad (17)$$

Since  $U_x < 0$  and  $\bar{p}_x > 0$  at the shock, the two sources of vorticity have the same sign if  $A_e$  and  $A_v$  have the same sign. In this case, the entropy wave enhances the amplification of vorticity across the shock. If the signs are opposite, the entropy wave weakens the vorticity amplification.

Using equation (17), we can derive an approximate expression for the value of the downstream vorticity in terms of its upstream value (see section 3.6 of Mahesh et al. 1996 for full derivation):

$$\omega_2' \sim \mathcal{C} \omega_1' + \frac{ik \sin \psi_1}{3} A_e U_1 \frac{1 - \mathcal{C}^3}{\mathcal{C}^2}, \quad (18)$$

where  $\mathcal{C}$  is the compression factor (12). This suggests that the incident vorticity wave amplifies by a factor of  $\mathcal{C}$  due to shock compression, while the vorticity created by the incident entropy wave is  $\propto k A_e \sin \psi_1 (1 - \mathcal{C}^3) / \mathcal{C}^2$ .

A word of caution is in order here. The effects due to the change of shock position and shape are absent in equation (18) and thus it has a limited quantitative accuracy. Nevertheless, as we will see below, it describes well some key qualitative aspects of our results.

In the limit of small incidence angle  $\psi_1$ , equation (18) yields  $\omega_2' \sim \mathcal{C} \omega_1'$ . For a  $\mathcal{M}_1 = 5$  shock,  $\mathcal{C} \simeq 5.6$ , which is precisely what we observe in Fig. 4 for  $\sqrt{\langle \omega_2'^2 \rangle} / \sqrt{\langle \omega_1'^2 \rangle}$  for all the three curves. As predicted by equation (18), the three curves gradually diverge with increasing  $\psi_1$ . Fig. 5 shows the vorticity amplification  $\sqrt{\langle \omega_2'^2 \rangle} / \sqrt{\langle \omega_1'^2 \rangle}$  for an incident vorticity wave across the shock as a function of angle  $\psi_1$  for various values of nuclear dissociation parameter  $\bar{\epsilon}$  for  $\mathcal{M}_1 = 5$ . Because of larger compression with increasing  $\bar{\epsilon}$ , the amplification  $\sqrt{\langle \omega_2'^2 \rangle} / \sqrt{\langle \omega_1'^2 \rangle}$  also grows with  $\bar{\epsilon}$ , in agreement with the prediction of equation (18).

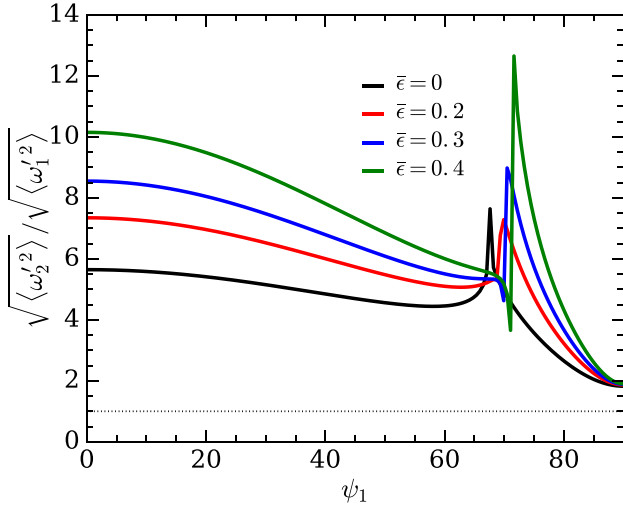


**Figure 5.** Amplification of vorticity across the shock as a function of angle  $\psi$  for various values of nuclear dissociation parameter  $\bar{e}$  for incident vorticity waves for  $\mathcal{M}_1 = 5$ . The horizontal dotted black line with  $y = 1$  is added as a reference line for a better readability of the plots.

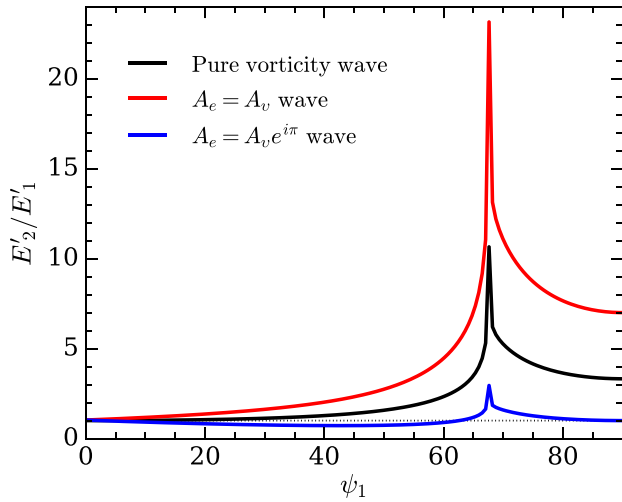


**Figure 6.** The amplification of turbulent kinetic energy across the shock with  $\mathcal{M}_1 = 5$  as a function of angle  $\psi$  for purely vorticity wave, in-phase vorticity–entropy wave (i.e.  $A_e = A_v$ ), and out-of-phase vorticity–entropy wave (i.e.  $A_e = A_v e^{i\pi}$ ). When the vorticity and entropy waves are in phase, we get the strongest amplification. When they are out of phase, there is no significant amplification. The horizontal dotted black line with  $y = 1$  is added as a reference line for better readability of the plots.

Fig. 6 shows the ratio of turbulent kinetic energy  $E'$  across the shock  $E'_2/E'_1$  as a function of angle  $\psi_1$  for  $\mathcal{M}_1 = 5$  and  $\bar{e} = 0$  for the same three types of incident perturbations. We define  $E'$  as

$$E' = \frac{1}{2} (\langle u'u'^* \rangle + \langle v'v'^* \rangle), \quad (19)$$

where  $\langle \rangle$  means averaging over  $t$  and  $y$ , while sign  $*$  denotes complex conjugate. Similarly to the case of  $\langle \omega'^2 \rangle$ , we observe the largest (smallest)  $E'_2/E'_1$  when entropy and vorticity waves are in phase (out of phase), while for pure vorticity wave,  $E'_2/E'_1$  is roughly the average of the two cases. For example, at  $\psi_1 = 60^\circ$ , for in-phase waves, we get  $E'_2/E'_1 = 4.51$ , while for out-of-phase waves, we get  $E'_2/E'_1 = 0.90$ , which means that the total kinetic

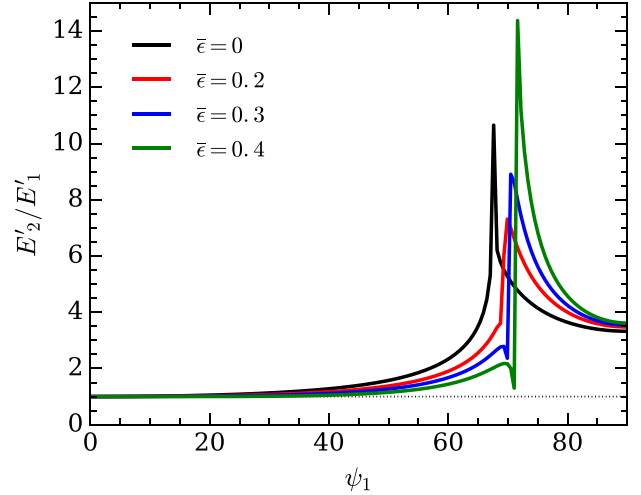


**Figure 7.** Amplification of turbulent kinetic energy across the shock as a function of angle  $\psi_1$  for various values of nuclear dissociation parameter  $\bar{e}$  for  $\mathcal{M}_1 = 5$  for incident vorticity waves. The horizontal dotted black line with  $y = 1$  is added as a reference line for a better readability of the plots.

energy of the perturbations actually decreases across the shock in this case for this value of  $\psi_1$ . For pure vorticity wave, we get  $E'_2/E'_1 = 2.36$  for the same  $\psi_1$ .

At  $\psi_1 \simeq 0$ , we see no amplification of  $E'$ , while the vorticity, as shown above, scales as  $\sqrt{\langle \omega'^2 \rangle} / \sqrt{\langle \omega_1^2 \rangle} \sim \mathcal{C}$ . This is due to the fact that in this limit, the  $x$ -component of the velocity perturbation  $u'_1 \simeq 0$ , while  $v'_1 \simeq A_v$ , i.e. the velocity perturbation has only a  $y$ -component, which is tangential to the shock. The tangential component of the velocity does not change across the shock (Landau & Lifshitz 1959). Hence, there is no amplification of turbulent kinetic energy in this limit. On the other hand, the vorticity  $\omega'$  still changes because it depends on the wavelength, which decreases by a factor given by equation (14).

The  $x$ -component of velocity of incident the vorticity wave grows with  $\psi_1$  as  $u'_1 \propto \sin \psi_1$  (cf. equation 2). The shock responds sensitively to  $u'_1$  by changing its position and shape according to equation (6). Because of the deformation of the shock, both  $x$ - and  $y$ -components of velocity will be perpendicular to the shock at some  $y$  and  $t$ . In this case, both  $u'$  and  $v'$  undergo significant amplifications across the shock. The amplification factor gradually grows with  $\psi_1$  reaching, e.g.  $\simeq 1.4$  and  $\simeq 2.3$  for  $\psi_1 = 45^\circ$  for purely vorticity and in-phase entropy–vorticity waves, respectively. The largest amplification is reached at  $\psi_1 \simeq \psi_c$ , with amplification factors of  $\simeq 6.2$  and  $\simeq 13$  for these two cases. However, such a large amplification is confined to a narrow range of values of  $\psi_1$  around  $\psi_c$  with width  $\lesssim 5^\circ$ .

Fig. 7 shows the amplification of kinetic energy as a function of  $\psi_1$  for various values of nuclear dissociation parameter  $\bar{e}$ , ranging from 0 to 0.4. As we can see,  $E'_2/E'_1$  exhibits only minor change with  $\bar{e}$ . The spike in  $E'_2/E'_1$  around  $\psi_1 \simeq 69^\circ$ , which corresponds to the critical angle  $\psi_1 = \psi_c$ , shifts towards slightly higher  $\psi$  with  $\bar{e}$  due to the fact the  $\psi_c$  increases with  $\bar{e}$  (cf. Fig. 2).

Fig. 8 shows the ratio of the kinetic energy of the acoustic component to the total kinetic energy of the entire fluctuating velocity field as a function of the incidence angle  $\psi_1$  for  $\bar{e} = 0, 0.2, 0.3$ , and 0.4 for  $\mathcal{M}_1 = 5$ . This ratio can reach up to 0.08 around  $\psi \sim 50^\circ$ , which is a non-negligible amount.



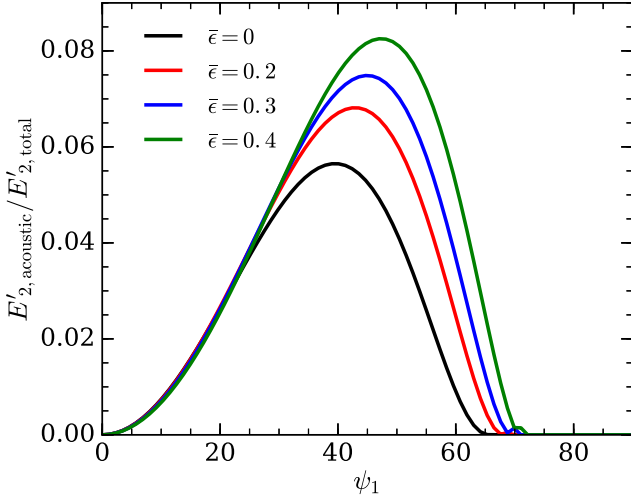


**Figure 8.** The ratio of kinetic energy associated with sound wave to the total kinetic energy of the fluctuating field in the post-shock region as a function of the incidence angle  $\psi_1$  for  $\mathcal{M}_1 = 5$  for incident vorticity waves.

### 3.2 Interaction with turbulence

So far, our analysis has focused on the interaction of shocks with individual fluctuation modes. In the following, we consider the interaction with turbulent fields, which we model as sets of random 3D vorticity and entropy waves. In the LIA, each of these waves interacts independently with the shock. The full turbulent statistics behind the shock can be obtained by integrating over the interactions of each of these waves with the shock.

In order to achieve this goal, we first need to establish how the 2D LIA presented so far is related to the general 3D problem. In 3D Cartesian coordinate system  $(x, y, z)$ , consider an incident planar wave with wavenumber  $\kappa_1$  that makes angle  $\psi_1$  with the  $x$ -axis. The latter is assumed to be perpendicular to the shock. The dynamics in the plane spanned by the vector  $\kappa_1$  and the shock normal is identical to that of the 2D LIA problem. The component of the velocity field perpendicular to this plane passes unchanged through the shock, while the components parallel to the plane change according to LIA (Ribner 1954; Mahesh et al. 1996; Wouchuk et al. 2009). In the following, we refer to this plane as the LIA plane.

We consider two types of turbulent fields. The first is an anisotropic turbulence characterized by relation

$$R_{rr} = R_{\theta\theta} + R_{\phi\phi} \quad \text{and} \quad R_{\theta\theta} = R_{\phi\phi}, \quad (20)$$

where  $R_{ij}$  is the  $ij$  component of the Reynolds stress tensor. This means an equipartition between radial and non-radial components of turbulent kinetic energy and it was observed in buoyancy-driven turbulent convection in stellar interiors (e.g. Arnett et al. 2009). The second type is a fully isotropic turbulence represented by

$$R_{rr} = R_{\theta\theta} = R_{\phi\phi}. \quad (21)$$

Estimate of how well equation (21) describes the turbulence in stellar convective shells is beyond the scope of this work. Instead, we use it as an alternative prescription in order to test the sensitivity of our results to the properties of upstream turbulence.

In order to model turbulence characterized by these relations, we randomly sample the velocity field  $(v_x, v_y, v_z)$  with a statistics that satisfies these relations. Here, the  $x$ -component  $v_x$  plays a role similar to that of the radial component in CCSNe since both of them are perpendicular to the shocks in their respective contexts. By the

same rationale,  $v_y$  and  $v_z$  play the roles of angular components in CCSNe.

The wavenumber vectors  $\kappa_1$  of incident waves are sampled randomly with uniform distribution on a 2D sphere. For each wave, we decompose the velocity field into three components: the first being perpendicular to the LIA plane, the second being perpendicular to  $\kappa_1$  on the LIA plane, and the third being parallel to  $\kappa_1$  on the LIA plane. The first component passes through the shock unchanged, while the second changes according to LIA. The third component represents the non-solenoidal part of the velocity field, which we set to zero when constructing the vorticity waves.

Using this velocity field, we first investigate how the spectrum of turbulence changes as it crosses the shock. Each turbulent eddy is characterized by its wavenumber  $\kappa$ . According to LIA, when a turbulent eddy with a wavenumber  $\kappa_1$  passes through the shock, the  $x$ -component of  $\kappa_1$  increases from  $\kappa_{1,x}$  to  $\mathcal{C}\kappa_{1,x}$ . The other two components,  $\kappa_{1,y}$  and  $\kappa_{1,z}$ , do not change. Thus, the wavenumber vector increases from

$$\kappa_1 = \sqrt{\kappa_{1,x}^2 + \kappa_{1,y}^2 + \kappa_{1,z}^2} \quad (22)$$

to

$$\kappa_2 = \sqrt{\mathcal{C}^2 \kappa_{1,x}^2 + \kappa_{1,y}^2 + \kappa_{1,z}^2} = \sqrt{(\mathcal{C} - 1)\kappa_{1,x}^2 + \kappa_1^2}. \quad (23)$$

Hence,

$$\frac{\kappa_2}{\kappa_1} = \sqrt{(\mathcal{C} - 1)\cos^2 \psi_1 + 1}, \quad (24)$$

where we used the definition  $\cos \psi_1 = \kappa_{1,x}/\kappa_1$ . Since  $\kappa = 2\pi/\lambda$ , where  $\lambda$  is the spatial scale of our eddy, the eddy becomes smaller by factor  $\kappa_2/\kappa_1$  as it passes through the shock. At most,  $\lambda$  can decrease by a factor of  $\mathcal{C}$ , which happens when  $\kappa_1$  is perpendicular to the shock. When  $\kappa_1$  is parallel to the shock, there is no change in the size of the eddy.

In order to obtain an average behaviour of  $\kappa_2/\kappa_1$ , we average it over a random set of vectors  $\kappa_1$  with uniform distribution on a 2D sphere. This is equivalent to sampling  $\cos \psi_1$  uniformly in interval  $[0, 1]$ , which, in turn, is equivalent to solving integral

$$\left\langle \frac{\kappa_2}{\kappa_1} \right\rangle = \int_0^1 \sqrt{(\mathcal{C} - 1)x + 1} \, dx. \quad (25)$$

The latter can be calculated analytically:

$$\left\langle \frac{\kappa_2}{\kappa_1} \right\rangle = \frac{2}{3} \frac{1 + \sqrt{\mathcal{C}} + \mathcal{C}}{1 + \sqrt{\mathcal{C}}}. \quad (26)$$

Fig. 9 shows the average ratio  $\langle \kappa_2/\kappa_1 \rangle$  as a function of nuclear dissociation parameter  $\bar{\epsilon}$  for four values of upstream Mach number: 2.4, 5, 10, and 100. In all cases,  $\langle \kappa_2/\kappa_1 \rangle$  increases mildly with  $\bar{\epsilon}$ . This is a simple reflection of the fact that the compression factor increases with  $\bar{\epsilon}$ , as we discussed above. For our fiducial values of  $\bar{\epsilon} = 0.2$  and  $\mathcal{M}_1 = 5$ ,  $\langle \kappa_2/\kappa_1 \rangle \simeq 2$ . As expected, this result does not change much with further increasing  $\mathcal{M}_1$ .

Now consider the post-shock turbulent kinetic energy. The total specific kinetic energy for a single wave is given by equation (19), which we rewrite as

$$E' = \frac{1}{2} (\langle u'^2 \rangle + \langle v'^2 \rangle), \quad (27)$$

where  $\langle u'^2 \rangle = \langle u'u'^* \rangle$ . For an incident vorticity–entropy wave of form (5), we obtain

$$E'_1 = \frac{1}{2} U_1^2 |A_v|^2. \quad (28)$$

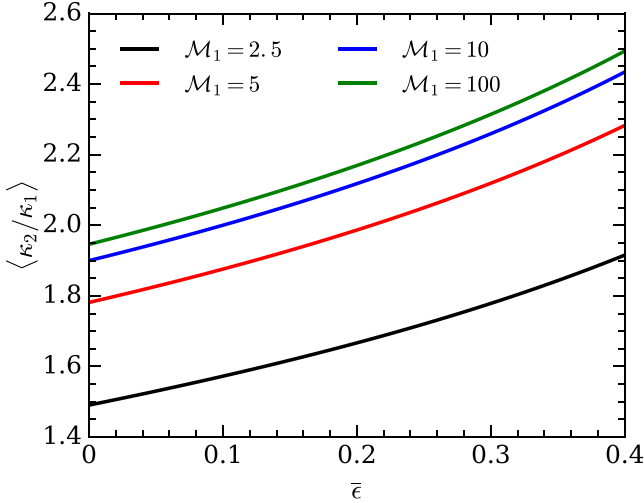


**Figure 9.** The average ratio of downstream and upstream wavenumbers of incident vorticity and/or entropy waves as a function of nuclear dissociation parameter  $\bar{\epsilon}$  for various values of upstream Mach number  $\mathcal{M}_1$ . For all the values of  $\bar{\epsilon}$  and  $\mathcal{M}_1$  considered here, the average wavenumber of the upstream turbulent field increases as it crosses the shock, meaning that the spectrum of the turbulent motion shifts towards smaller wavelengths.

For the downstream vorticity field (7) and (8), in the far-field region ( $x > 1/\kappa$ ), we have<sup>2</sup>

$$E'_2 = \frac{1}{2} U_1^2 (|G|^2 + |I|^2). \quad (29)$$

Thus, the ratio of upstream and downstream turbulent kinetic energies is

$$\frac{E'_2}{E'_1} = |\tilde{G}|^2 + |\tilde{I}|^2, \quad (30)$$

where  $\tilde{G} = G/A_v$  and  $\tilde{I} = I/A_v$ .

Note that formula (30) depends only on  $A_e/A_v$  and the incidence angle  $\psi_1$  of upstream vorticity–entropy waves, but not on their wavenumbers  $\kappa_1$ . This is an important result because it means that the amplification factor of turbulent kinetic energy across the shock is independent of the spectrum of upstream turbulence.

The black line in Fig. 10 shows the amplification of the total kinetic energy across the shock as a function of the nuclear dissociation parameter  $\bar{\epsilon}$  for incident vorticity waves. Here, we use an anisotropic turbulent field represented by relation (20) and each point on this graph is calculated using a sample of 150 000 random incident waves. The amplification of the total energy  $E'_2/E'_1$  does not change much with  $\bar{\epsilon}$ , remaining at  $\simeq 2.14$  as  $\bar{\epsilon}$  grows from 0 to 0.4. On the other hand, the amplification of the angular and radial components, defined as  $(E'_{y,2} + E'_{z,2})/(E'_{y,1} + E'_{z,1})$  and  $E'_{x,2}/E'_{x,1}$ , exhibit noticeable dependence on  $\bar{\epsilon}$ . The angular component, shown with the red line in Fig. 10, increases from 2.85 to 3.15 as  $\bar{\epsilon}$  grows from 0 to 0.4. Contrary to this, the amplification of the radial component, shown with the blue line in Fig. 10, decreases from 1.30 to 0.90 for the same values of  $\bar{\epsilon}$ .

<sup>2</sup> Note that equation (29) does not include the contribution from acoustic waves. In order to include that, we would have to add  $\frac{1}{2} U_1^2 (|F|^2 + |H|^2)$  to the right-hand side of equation (29) in the propagative regime ( $\psi_1 < \psi_c$ ). In the non-propagative regime, there is no contribution from the acoustic component.

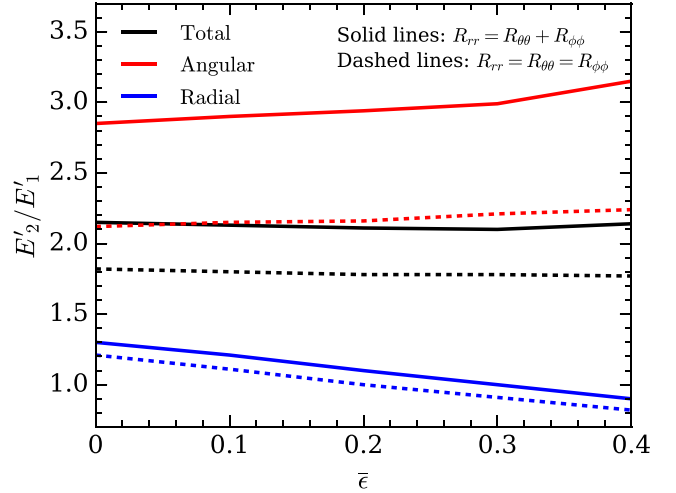


**Figure 10.** The amplification of turbulent kinetic energy across the shock as a function of nuclear dissociation parameter  $\bar{\epsilon}$  for incident vorticity waves. The black line represents the amplification of the total kinetic energy, while red and blue lines represent the amplifications of angular and radial components of the kinetic energy. The solid lines correspond to anisotropic turbulence represented by relation  $R_{rr} = R_{\theta\theta} + R_{\phi\phi}$ , while the dashed lines correspond to fully isotropic turbulence represented by relation  $R_{rr} = R_{\theta\theta} = R_{\phi\phi}$ .

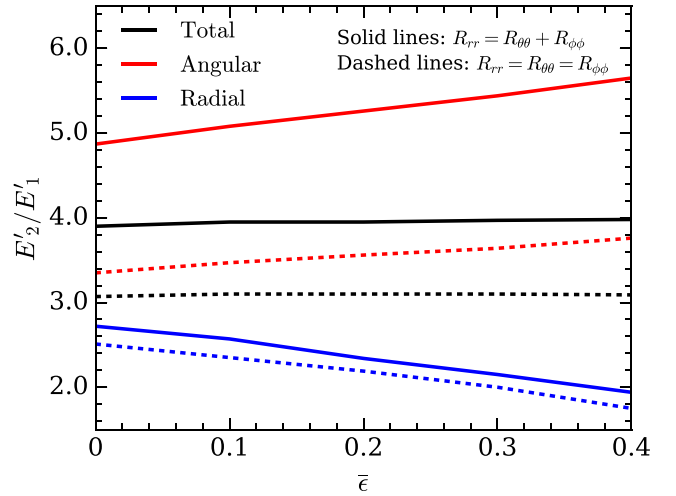


**Figure 11.** The amplification of turbulent kinetic energy across the shock as a function of nuclear dissociation parameter  $\bar{\epsilon}$  for incident entropy vorticity waves of the same phase. The black line represents the amplification of the total kinetic energy, while red and blue lines represent the amplifications of angular and radial components of the kinetic energy. The solid lines correspond to anisotropic turbulence represented by relation  $R_{rr} = R_{\theta\theta} + R_{\phi\phi}$ , while the dashed lines correspond to fully isotropic turbulence represented by relation  $R_{rr} = R_{\theta\theta} = R_{\phi\phi}$ .

Similar to the behaviour of individual waves discussed earlier in Section 3.1, the change of kinetic energy of the incident vorticity waves across the shock is very sensitive to the presence of incident entropy waves. If we add entropy waves with the same phase and amplitude as the incident vorticity waves (i.e.  $A_e = A_v$ ), the amplification of total kinetic energy of turbulent field becomes  $\simeq 3.95$  (cf. the dashed black line in Fig. 11). This is  $\simeq 1.85$  times larger than what we get in the case of pure vorticity waves shown in Fig. 10. On the other hand, if they are out of phase (i.e.  $A_e = A_v e^{i\pi}$ ), we

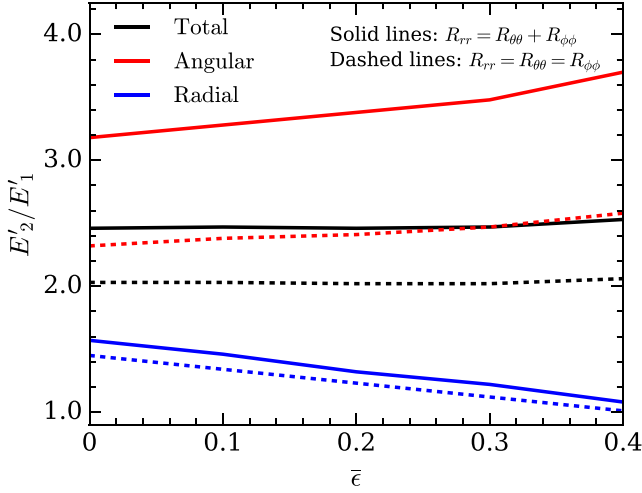


**Figure 12.** The amplification of turbulent kinetic energy across the shock as a function of nuclear dissociation parameter  $\bar{\epsilon}$  for incident entropy and vorticity waves. The phase difference between the two waves are chosen randomly with a uniform distribution in  $(0, 2\pi)$ . The black line represents the amplification of the total kinetic energy, while red and blue lines represent the amplifications of angular and radial components of the kinetic energy. The solid lines correspond to anisotropic turbulence represented by relation  $R_{rr} = R_{\theta\theta} + R_{\phi\phi}$ , while the dashed lines correspond to fully isotropic turbulence represented by relation  $R_{rr} = R_{\theta\theta} = R_{\phi\phi}$ .

find that the total energy does not change much and  $E'_2/E'_1 \sim 1$  (not shown here). Such a dependence on entropy waves is a direct manifestation of the simple scaling law (18) discussed above.

We also consider the case when the phase difference between the incident entropy and vorticity waves are chosen randomly with uniform distribution between 0 and  $2\pi$ . This case is presented in Fig. 12. We find that in this case, the overall behaviour of the turbulent kinetic energy is qualitatively and quantitatively similar to that in the case of incident pure vorticity waves shown in Fig. 10. For fiducial parameters,  $\mathcal{M}_1 = 5$  and  $\bar{\epsilon} = 0.2$ , we get  $E'_2/E'_1 = 2.46$ ,  $(E'_{y,2} + E'_{z,2})/(E'_{y,1} + E'_{z,1}) = 3.38$ , and  $E'_{x,2}/E'_{x,1} = 1.32$ .

We can summarize these findings as follows. If the phases of incident entropy and vorticity are strongly correlated, then the total kinetic energy of the turbulent field will increase by a factor of  $\sim 4$ . If they are strongly anticorrelated, then there is no amplification. If there is no correlation in the phases, then the amplification is  $\sim 2$ .

In order to test the sensitivity of our results to the particular form of (20), we repeat this exercise for isotropic turbulence represented by equation (21). The dashed black lines in Figs 10 and 11 show the amplification of the total turbulent kinetic energy of the field of incident vorticity and in-phase entropy–vorticity waves, respectively. In both cases, the amplification is again insensitive to  $\bar{\epsilon}$ , remaining at  $\sim 1.8$  and  $\sim 3.1$  for incident vorticity and in-phase entropy–vorticity waves. These values are  $\sim 15$  and  $\sim 21$  percent smaller than those in the case of anisotropic turbulence. Despite similarity of the behaviour of the total energy across the shock, we see differences in the behaviour of radial and angular components.

For isotropic turbulence, the amplification factors of the angular and radial components are closer to each other than those for the anisotropic turbulence. For example, for  $\bar{\epsilon} = 0.2$  and incident vorticity wave, the ratios of the amplifications of angular and radial components are 2.67 and 2.16 for anisotropic and isotropic turbulence models. The reason for larger amplification of angular component in anisotropic turbulence is due to the fact that a smaller

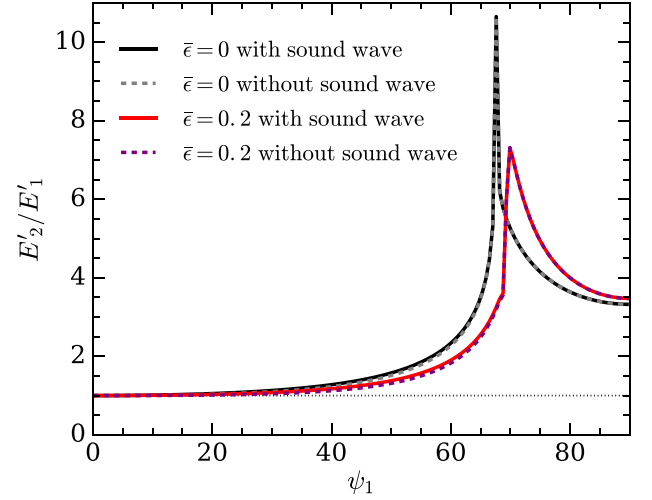


**Figure 13.** The ratios of upstream and downstream kinetic energies of turbulent field as a function of the incidence angle  $\psi_1$  for  $\mathcal{M}_1 = 5$  for incident vorticity waves. The solid lines include the contribution of sound waves to the kinetic energy, while the dashed lines do not. The horizontal dotted black line with  $y = 1$  is added as a reference line for a better readability of the plots.

fraction of the kinetic energy is contained in a component tangential to the shock, which does not undergo amplification.

Our analysis shows that, downstream of the shock, acoustic waves contribute at most  $\sim 2$  per cent of the total turbulent kinetic energy, which is a tiny amount. This may seem surprising in the light of the fact that the ratio of the kinetic energy of sound waves to the kinetic energy of the total fluctuating velocity field can reach  $\sim 0.08$  for  $\psi \sim 50^\circ$ , as we saw in Fig. 8. However, the total kinetic energy of the fluctuating field in this region is small compared to that at larger  $\psi$ . This is easily visible in Fig 13, which shows, for incident vorticity waves, the ratio of upstream and downstream kinetic energies with and without the contribution of the downstream acoustic field with solid and dashed lines, respectively. As we can see, if we average over all values of  $\psi_1$ , the contribution of the acoustic component should be negligibly small, in agreement with our findings above.

The shock surface responds to upstream velocity perturbations by oscillating according to formula (6). Fig. 14 shows the normalized rms velocity of the shock  $\sqrt{\langle \xi_r^2 \rangle / \langle u_1^2 \rangle}$  as a function of nuclear dissociation parameter  $\bar{\epsilon}$  for  $\mathcal{M}_1 = 5$ . Here,  $\langle u_1^2 \rangle$  is the rms value of the  $x$ -component of the perturbation velocity. The black line corresponds to incident vorticity waves, while the red and blue lines correspond to incident entropy and vorticity waves with the same phase (i.e.  $A_e = A_v$ ) and  $180^\circ$  phase difference ( $A_e = A_v e^{i\pi}$ ), respectively. Finally, the green line represents the case where the entropy and vorticity waves have randomly sampled phase differences from 0 to  $2\pi$  with uniform distribution (i.e.  $A_e = A_v e^{i\pi r}$ , where  $r$  is a random number with uniform distribution in  $[0, 2]$ ). Similar to the amplification of turbulent kinetic energy, the shock velocity does not change much with  $\bar{\epsilon}$ , but it is very sensitive to the presence of entropy waves. For our fiducial value  $\bar{\epsilon} = 0.2$ , we get the largest  $\sqrt{\langle \xi_r^2 \rangle / \langle u_1^2 \rangle}$  of  $\sim 0.8$  for  $A_e = A_v$ , while for case  $A_e = A_v e^{i\pi}$ , we get the smallest  $\sqrt{\langle \xi_r^2 \rangle / \langle u_1^2 \rangle}$  of  $\sim 0.2$ . In the case of incident entropy–vorticity waves with randomly distributed phase differences and in the case of incident vorticity waves, we get similar values of  $\sqrt{\langle \xi_r^2 \rangle / \langle u_1^2 \rangle} \sim 0.58$  and  $\sim 0.47$ , respectively. Note that, due to the



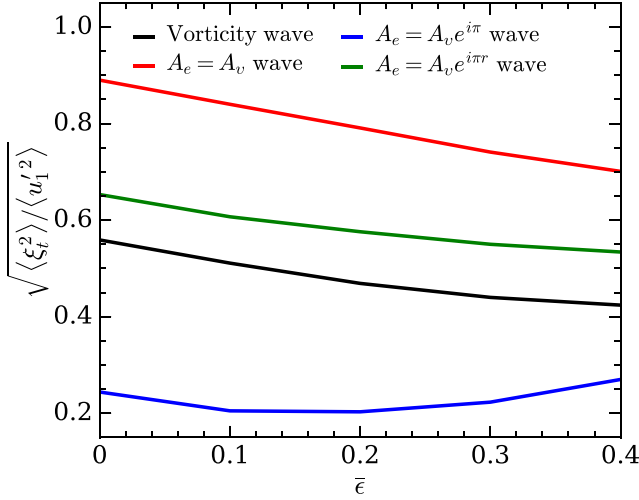


**Figure 14.** The normalized rms velocity of the shock oscillations  $\sqrt{\langle \xi_t^2 \rangle / \langle u_1'^2 \rangle}$  as a function of nuclear dissociation parameter  $\bar{\epsilon}$  for  $\mathcal{M}_1 = 5$ . The black line corresponds to incident vorticity waves, while the red and blue lines correspond to incident entropy and vorticity waves with the same phase (i.e.  $A_e = A_v$ ) and  $180^\circ$  phase difference ( $A_e = A_v e^{i\pi}$ ), respectively. Finally, the green line represents the case where the entropy and vorticity waves have randomly sampled phase differences from 0 to  $2\pi$  with uniform distribution (i.e.  $A_e = A_v e^{i\pi r}$  where  $r \in [0, 2]$  is random number). We get the strongest velocities  $\sqrt{\langle \xi_t^2 \rangle / \langle u_1'^2 \rangle}$  of  $\sim 0.8$  in the case of in-phase entropy–vorticity waves. When they are out of phase, we get the weakest amplification  $\sqrt{\langle \xi_t^2 \rangle / \langle u_1'^2 \rangle} \sim 0.2$ . In the case of randomly distributed phase differences and in the case of incident vorticity waves, we get similar values of  $\sqrt{\langle \xi_t^2 \rangle / \langle u_1'^2 \rangle}$  of  $\sim 0.58$  and  $\sim 0.47$ , respectively.

employed normalization, these values do not depend on whether we use anisotropic (equation 20) or isotropic (equation 21) turbulence prescriptions.

#### 4 IMPLICATIONS FOR THE EXPLOSION CONDITION

We now discuss the implications of the above results on the conditions for producing explosion using the concept of critical luminosity (Burrows & Goshy 1993). According to Müller & Janka (2015), in the presence of post-shock turbulence, the critical luminosity for producing explosion is

$$L_v E_v^2 \propto (\dot{M} M)^{3/5} r_{\text{gain}}^{-2/5} \left( 1 + \frac{4 \langle \mathcal{M}_2'^2 \rangle}{3} \right)^{-3/5}, \quad (31)$$

where  $\langle \mathcal{M}_2'^2 \rangle$  is the rms post-shock turbulent Mach number. Following Müller & Janka (2015), we define it as

$$\langle \mathcal{M}_2'^2 \rangle = \frac{\langle v_a^2 \rangle}{\langle c_s^2 \rangle}, \quad (32)$$

where  $\langle v_a^2 \rangle$  is rms angular velocity, which can be expressed in terms of specific kinetic energy of angular turbulent motion as  $\langle v_a^2 \rangle = 2E'_a$ . Using this, we can write

$$\langle \mathcal{M}_2'^2 \rangle = \frac{2E'_{a,2}}{\langle c_s^2 \rangle} = 2 \frac{E'_{a,2}}{E'_{a,1}} \frac{E'_{a,1}}{\langle c_s^2 \rangle} = \frac{E'_{a,2}}{E'_{a,1}} \frac{\langle v_{a,1}^2 \rangle}{\langle c_{s,2}^2 \rangle} = \frac{E'_{a,2}}{E'_{a,1}} \frac{\langle c_{s,1}^2 \rangle}{\langle c_{s,2}^2 \rangle} \langle \mathcal{M}_1'^2 \rangle. \quad (33)$$

Substituting this into equation (31), we get

$$L_v E_v^2 \propto \left( 1 + \frac{4}{3} \frac{E'_{a,2}}{E'_{a,1}} \frac{\langle c_{s,1}^2 \rangle}{\langle c_{s,2}^2 \rangle} \langle \mathcal{M}_1'^2 \rangle \right)^{-3/5} \\ \simeq 1 - \frac{4}{5} \frac{E'_{a,2}}{E'_{a,1}} \frac{\langle c_{s,1}^2 \rangle}{\langle c_{s,2}^2 \rangle} \langle \mathcal{M}_1'^2 \rangle. \quad (34)$$

Note that we linearized in  $\langle \mathcal{M}_1'^2 \rangle$  in the last step. Subtracting this from the critical luminosity in the absence of post-shock turbulence, we obtain an expression for the relative reduction of the critical luminosity due to upstream turbulence:

$$\delta(L_v E_v^2) \simeq \frac{4}{5} \frac{E'_{a,2}}{E'_{a,1}} \frac{\langle c_{s,1}^2 \rangle}{\langle c_{s,2}^2 \rangle} \langle \mathcal{M}_1'^2 \rangle. \quad (35)$$

For our fiducial parameters  $\bar{\epsilon} = 0.2$  and  $\mathcal{M}_1 = 5$ ,  $\langle c_{s,1}^2 \rangle / \langle c_{s,2}^2 \rangle \simeq 0.25$  and  $E'_{a,2} / E'_{a,1} \sim 3$  for anisotropic turbulence represented by relation (20) for an incident field of vorticity or entropy–vorticity waves with uncorrelated phases. For these values, equation (35) reduces to

$$\delta(L_v E_v^2) \simeq 0.6 \langle \mathcal{M}_1'^2 \rangle. \quad (36)$$

Thus, the critical luminosity decreases by  $\simeq 0.6 \langle \mathcal{M}_1'^2 \rangle$  compared to the case with no post-shock turbulence.

In convective shells, we expect  $\sqrt{\langle \mathcal{M}'^2 \rangle} \sim 0.1$  (e.g. Müller et al. 2016). During collapse, the Mach number of non-radial fluctuations increases as  $\propto r^{(3\gamma - 7)/4}$  (Lai & Goldreich 2000). Assuming that convective shells fall from a radius of  $\sim 1500$  to  $\sim 200$  km before it hits the shock, in the absence of turbulent dissipation, the turbulent Mach number should increase to  $\sim 0.45$  before hitting the shock, which yields  $\langle \mathcal{M}'^2 \rangle \sim 0.21$ . This results in a reduction of the critical luminosity by  $\sim 12$  per cent compared to the case with no upstream turbulence.

Note that the estimate (36) is of limited accuracy for a number of reasons. First, it neglects turbulent dissipation in the post-shock region. Second, it is based on a comparison to the hypothetical case with no post-shock turbulence. However, by the time a nuclear-burning shell hits the shock, the post-shock region is expected to have a fully developed neutrino-driven turbulent convection (Couch et al. 2015), which we cannot include in our estimate. Both of these effects overestimate the reduction of critical luminosity.

Another important effect that is missing in our analysis is the gravitational potential energy of turbulent eddies crossing the shock. As the eddies move downstream, part of their gravitational potential energy is converted into kinetic energy of the post-shock non-radial motion by buoyancy forces. Recently, Müller et al. (2016) provided an order-of-magnitude estimate of the decrease of the critical luminosity due to this effect. For a  $18 M_\odot$  progenitor model with a convective Mach number of 0.1, they find that the critical luminosity decreases by 12 and 24 per cent for  $\ell = 4$  and 2 perturbations. In the framework of our model, we cannot include this effect rigorously, but it is reasonable to expect that this effect may further reduce the critical luminosity by extra few per cent.

#### 5 CONCLUSION

In this paper, we studied the interaction of the shock waves in CC-SNe with turbulent convection arising from nuclear shell burning. We used a first-order perturbation theory called the LIA, which we extended to include nuclear dissociation at the shock. In the LIA, the shock wave is modelled as a planar discontinuity with no intrinsic scale. The upstream flow, which consists of mean and

fluctuating part, fully determines the downstream flow via the Rankine–Hugoniot conditions at the shock. In the LIA, the turbulent field is decomposed into individual Fourier modes. Each mode interacts independently with the shock. Integration over all modes yields the full statistics of the turbulent flow (cf. Section 2).

In order to approximate the situation in CCSNe, we required the mean flow to have the vanishing Bernoulli parameter in the pre-shock region. We considered two types of upstream incident perturbations: the vorticity and entropy waves, both of which are advected with the mean flow. The vorticity mode is a solenoidal velocity field that has no pressure or density fluctuations, while the entropy mode represents density and temperature fluctuations with no associated pressure or velocity variations. Once the incident perturbations hit the shock, the downstream fluctuation field consists of vorticity, entropy, and acoustic waves (cf. Section 2).

The compression factor  $\mathcal{C}$  at the shock is the key quantity that affects the flow through the shock. In particular, it determines by how much the  $x$ -component of the wavenumber of incident waves increase as they cross the shock. Nuclear dissociation leads to stronger compression:  $\mathcal{C}$  increases from 5.56 to 10.15 as nuclear dissociation parameter  $\bar{\epsilon}$  increases from 0 (inefficient nuclear dissociation) to 0.4 (efficient nuclear dissociation). The compression factor  $\mathcal{C}$  grows fast with the upstream Mach number  $\mathcal{M}_1$  until  $\mathcal{M}_1 \sim 5$ , after which it does not change much with further increase of  $\mathcal{M}_1$ . We find most of the quantities that characterize the downstream perturbation field have a similar dependence on  $\mathcal{M}_1$  for  $\mathcal{M}_1 \gtrsim 5$  (cf. Section 3).

The critical angle  $\psi_c$  separates two regions of the solution:  $\psi_1 < \psi_c$  and  $\psi_1 > \psi_c$ , where  $\psi_1$  is the incidence angle. The  $\psi_1 < \psi_c$  region is called the propagative regime and it is characterized by acoustic waves in the post-shock flow, while  $\psi_1 > \psi_c$  is called the non-propagative region, in which sound waves do not propagate. We investigated how  $\psi_c$  depends on the free parameters of the mean flow: the upstream Mach number  $\mathcal{M}_1$  and the efficiency of nuclear dissociation (cf. Section 2). We find that  $\psi_c$  depends weakly on both of these parameters. For our fiducial parameters, we get  $\psi_c = 69.2^\circ$  (cf. Section 3).

We explored how individual vorticity and entropy waves affect the shock and the downstream flow (Section 3.1). In particular, we analysed the amplification of the kinetic energy of individual incident waves as they cross the shock. The amplification of kinetic energy does not change much with  $\bar{\epsilon}$  and  $\mathcal{M}_1$  for  $\mathcal{M}_1 \gtrsim 5$ . On the other hand, it is highly sensitive to the relative phase between the entropy and vorticity waves: when they are in phase, we get the strongest amplification, while when they are out of phase, the kinetic energy does not amplify much. In fact, it may even decrease for some values of  $\psi_1$ . For example, for our fiducial parameters,  $\mathcal{M}_1 = 5$  and  $\bar{\epsilon} = 5$ , we get the amplification factors of 4.51 and 0.90 for in-phase and out-of-phase entropy–vorticity waves for  $\psi_1 = 60^\circ$ . The amplification for incident vorticity waves is roughly the average of these two regimes. For example, for the same values of  $\bar{\epsilon}$ ,  $\mathcal{M}_1$ , and  $\psi_1$ , we get an amplification of 2.36 (cf. Section 3.1).

For an incident field of turbulent fluctuations, we calculated the amplification of total turbulent kinetic energy. We find that the amplification is not sensitive to the nuclear dissociation parameter and the upstream Mach number beyond  $\mathcal{M}_1 \gtrsim 5$ . We again observe strong dependence on the phase difference between the incident vorticity and entropy waves. When they are in phase, the total kinetic energy increases by a factor of  $\sim 4$ , while when they are out of phase, there is almost no amplification. When the phase is randomly distributed, the amplification is  $\sim 2$ . When there is only incident vorticity wave perturbations, the amplification is again  $\sim 2$  (cf. Section 3.2).

When a turbulent eddy crosses the shock, it shrinks in size due to shock compression. We find that for our fiducial values, the average linear size of a turbulent eddy shrinks by a factor of  $\simeq 2$  (cf. Section 3.2). This value does not change much with the upstream Mach number  $\mathcal{M}_1$  and the nuclear dissociation parameter. This is somewhat disappointing news from the point of producing explosion because smaller eddies are perhaps less likely to become buoyant and help explosion (e.g. Couch 2013).

When a turbulent field crosses the shock, the post-shock turbulence exerts additional pressure behind the shock. This reduces the critical neutrino luminosity necessary to drive the explosion (Müller & Janka 2015). We find that, compared to the case with no post-shock turbulence, the critical luminosity decreases by a factor of  $\simeq 0.6 \langle \mathcal{M}_1^2 \rangle$ , where  $\langle \mathcal{M}_1^2 \rangle$  is the rms turbulent Mach number in the pre-shock region. If the turbulent Mach number in convective shells is  $\sim 0.1$ , it may increase to  $\langle \mathcal{M}_1^2 \rangle \sim 0.21$  during collapse prior to hitting the shock. This results in  $\sim 12$  per cent reduction in the critical luminosity (cf. Section 4).

## ACKNOWLEDGEMENTS

We thank our referee, Thierry Foglizzo, for fruitful discussions and a thorough review that improved this paper. We also thank Jim Fuller and Bernhard Müller for valuable discussions and comments. This work is partially supported by ORAU and Social Policy grants at Nazarbayev University and by the Sherman Fairchild Foundation.

## REFERENCES

- Abdikamalov E. et al., 2015, *ApJ*, 808, 70
- Arnett D., Meakin C., Young P. A., 2009, *ApJ*, 690, 1715
- Blondin J. M., Mezzacappa A., DeMarino C., 2003, *ApJ*, 584, 971
- Bruenn S. W. et al., 2016, *ApJ*, 818, 123
- Burrows A., 2013, *Rev. Modern Phys.*, 85, 245
- Burrows A., Goshy J., 1993, *ApJ*, 416, L75
- Burrows A., Hayes J., Fryxell B. A., 1995, *ApJ*, 450, 830
- Cardall C. Y., Budiardja R. D., 2015, *ApJ*, 813, L6
- Chang C.-T., 1957, *J. Aeronautical Sci.*, 24, 675
- Chatzopoulos E., Couch S. M., Arnett W. D., Timmes F. X., 2016, *ApJ*, 822, 61
- Couch S. M., 2013, *ApJ*, 775, 35
- Couch S. M., Ott C. D., 2013, *ApJ*, 778, L7
- Couch S. M., Ott C. D., 2015, *ApJ*, 799, 5
- Couch S. M., Chatzopoulos E., Arnett W. D., Timmes F. X., 2015, *ApJ*, 808, L21
- Dolence J. C., Burrows A., Murphy J. W., Nordhaus J., 2013, *ApJ*, 765, 110
- Duck P. W., Lasseigne D. G., Hussaini M. Y., 1997, *Phys. Fluids*, 9, 456
- Fabre D., Jacquin L., Sesterhenn J., 2001, *Phys. Fluids*, 13, 2403
- Fernández R., 2015, *MNRAS*, 452, 2071
- Fernández R., Thompson C., 2009a, *ApJ*, 697, 1827
- Fernández R., Thompson C., 2009b, *ApJ*, 703, 1464
- Foglizzo T., Scheck L., Janka H.-T., 2006, *ApJ*, 652, 1436
- Foglizzo T., Galletti P., Scheck L., Janka H.-T., 2007, *ApJ*, 654, 1006
- Foglizzo T. et al., 2015, *Publ. Astron. Soc. Aust.*, 32, e009
- Hanke F., Marek A., Müller B., Janka H.-T., 2012, *ApJ*, 755, 138
- Hanke F., Müller B., Wongwathanarat A., Marek A., Janka H.-T., 2013, *ApJ*, 770, 66
- Herant M., 1995, *Phys. Rep.*, 256, 117
- Huete Ruiz de Lira C., Velikovich A. L., Wouchuk J. G., 2011, *Phys. Rev. E*, 83, 056320
- Huete C., Wouchuk J. G., Velikovich A. L., 2012, *Phys. Rev. E*, 85, 026312
- Huete C., Sánchez A. L., Williams F. A., 2013, *Phys. Fluids*, 25, 076105
- Huete C., Sánchez A. L., Williams F. A., 2014, *Phys. Fluids*, 26, 116101
- Jackson T. L., Kapila A. K., Hussaini M. Y., 1990, *Phys. Fluids A*, 2, 1260
- Janka H.-T., Müller E., 1996, *A&A*, 306, 167

- Janka H.-T., Hanke F., Hudepohl L., Marek A., Müller B., Obergaulinger M., 2012, *Progress Theor. Exp. Phys.*, 2012, 010000
- Janka H.-T., Melson T., Summa A., 2016, preprint (arXiv:1602.05576)
- Kovaszny L. S. G., 1953, *J. Aeronautical Sci.*, 20, 657
- Lai D., Goldreich P., 2000, *ApJ*, 535, 402
- Landau L. D., Lifshitz E. M., 1959, *Fluid Mechanics*, 2nd edn. Butterworth-Heinemann, Oxford
- Lee S., Lele S. K., Moin P., 1993, *J. Fluid Mech.*, 251, 533
- Lentz E. J. et al., 2015, *ApJ*, 807, L31
- McKenzie J. F., Westphal K. O., 1968, *Phys. Fluids*, 11, 2350
- Mahesh K., Moin P., Lele S. K., 1996, Technical Report TF-69, The Interaction of a Shock Wave with a Turbulent Shear Flow. Thermosciences Division, Department of Mechanical Engineering, Stanford University
- Mahesh K., Lele S. K., Moin P., 1997, *J. Fluid Mech.*, 334, 353
- Melson T., Janka H.-T., Marek A., 2015a, *ApJ*, 801, L24
- Melson T., Janka H.-T., Bollig R., Hanke F., Marek A., Müller B., 2015b, *ApJ*, 808, L42
- Moore F. K., 1954, Technical Report TR 1165, Unsteady Oblique Interaction of a Shock Wave with a Plane Disturbance. NACA
- Müller B., Janka H.-T., 2015, *MNRAS*, 448, 2141
- Müller B., Viallet M., Heger A., Janka H.-T., 2016, *ApJ*, preprint (arXiv:1605.01393)
- Murphy J. W., Dolence J. C., Burrows A., 2013, *ApJ*, 771, 52
- Ott C. D. et al., 2013, *ApJ*, 768, 115
- Radice D., Couch S. M., Ott C. D., 2015, *Comput. Astrophys. Cosmol.*, 2, 7
- Radice D., Ott C. D., Abdikamalov E., Couch S. M., Haas R., Schnetter E., 2016, *ApJ*, 820, 76
- Ribner H. S., 1953, Technical Report TN 2864, Convection of a Pattern of Vorticity Through a Shock Wave. NACA
- Ribner H. S., 1954, Technical Report TN 3255, Shock-Turbulence Interaction and the Generation of Noise. NACA
- Roberts L. F., Ott C. D., Haas R., O'Connor E. P., Diener P., Schnetter E., 2016, *ApJ*, preprint (arXiv:1604.07848)
- Ryu J., Livescu D., 2014, *J. Fluid Mech.*, 756, R1
- Sagaut P., Cambon C., 2008, *Homogeneous Turbulence Dynamics*. Cambridge Univ. Press, Cambridge, doi: http://dx.doi.org/10.1017/CBO9780511546099
- Takahashi K., Yamada S., 2014, *ApJ*, 794, 162
- Takiwaki T., Kotake K., Suwa Y., 2014, *ApJ*, 786, 83
- Wouchuk J. G., Huete Ruiz de Lira C., Velikovich A. L., 2009, *Phys. Rev. E*, 79, 066315

## APPENDIX A: NUCLEAR DISSOCIATION AND THE SHOCK COMPRESSION FACTOR

We choose our one-dimensional (1D) shock parameters to approximate the CCSN shock by assuming vanishing Bernoulli parameter above the shock:

$$B \equiv \frac{1}{2}v_1^2 + \frac{\gamma p_1}{(\gamma - 1)\rho_1} - \frac{GM}{R} = 0, \quad (\text{A1})$$

where  $v_1$  represents the radial velocity immediately above the shock. We use  $\gamma = 4/3$  in all of our calculations. From equation (A1), we get

$$\frac{GM}{R} = \frac{1}{2}v_1^2 + \frac{\gamma p_1}{(\gamma - 1)\rho_1} = \frac{1}{2}v_1^2 + \frac{c_{s,1}^2}{\gamma - 1}, \quad (\text{A2})$$

where  $c_{s,1}$  is the speed of sound in the pre-shock region. Using the free-fall velocity,  $v_{\text{ff}}^2 = 2GM/R$ , we rewrite the above equation as

$$v_{\text{ff}}^2 = v_1^2 + \frac{2c_{s,1}^2}{\gamma - 1}. \quad (\text{A3})$$

Following Fernández & Thompson (2009a), Fernández & Thompson (2009b) and Radice et al. (2016), we parametrize  $\epsilon$  as

$$\epsilon = \bar{\epsilon} \frac{1}{2}v_{\text{ff}}^2, \quad (\text{A4})$$

where  $\bar{\epsilon}$  is a dimensionless parameter that typically ranges from 0.2 to 0.4 (Fernández & Thompson 2009a,b). Using this definition, we can write the following expression for nuclear dissociation energy:

$$\epsilon = \frac{1}{2}\bar{\epsilon} \left[ v_1^2 + \frac{2c_{s,1}^2}{\gamma - 1} \right]. \quad (\text{A5})$$

Our nuclear dissociation model affects the shock and the LIA formalism by affecting the compression factor  $\mathcal{C}$ . The latter is given by (Fernández & Thompson 2009a)

$$\mathcal{C} = \frac{\gamma + 1}{\gamma + \frac{1}{M_1^2} - \sqrt{\left(1 - \frac{1}{M_1^2}\right)^2 + (\gamma^2 - 1)\frac{2\epsilon}{v_1^2}}}, \quad (\text{A6})$$

which depends on nuclear dissociation via the term  $2\epsilon/v_1$ . This, in turn, can be obtained from equation (A5):

$$\frac{2\epsilon}{v_1^2} = \bar{\epsilon} \left[ 1 + \frac{2}{\gamma - 1} \frac{1}{\mathcal{M}_1} \right]. \quad (\text{A7})$$

Substituting this into equation (A6), we get equation (12) for  $\mathcal{C}$ :

$$\mathcal{C} = \frac{\gamma + 1}{\gamma + \frac{1}{M_1^2} - \sqrt{\left(1 - \frac{1}{M_1^2}\right)^2 + (\gamma + 1)\frac{(\gamma - 1)\mathcal{M}_1^2 + 2}{\mathcal{M}_1^2}\bar{\epsilon}}}. \quad (\text{A8})$$

Note that this equation depends only on the upstream Mach number  $\mathcal{M}_1$  and the nuclear dissociation parameter  $\bar{\epsilon}$ . We fix our units by setting  $\rho_1 = v_1 = 1$ , which leaves us with only two free parameters,  $\mathcal{M}_1$  and  $\bar{\epsilon}$ , that fully specify the mean flow.

## APPENDIX B: THE LIA FORMALISM

For completeness, we present the LIA formalism in this section. Our presentation, including notation, closely follows that of Mahesh et al. (1996). The shock wave is modelled as planar discontinuity. The flow is decomposed into the mean and fluctuating parts. The latter is assumed to be weak so that the mean flow obeys the usual Rankine–Hugoniot conditions, while the perturbations obey the linearized version. The upstream flow completely determines the downstream flow and the shock dynamics.

We start with the Rankine–Hugoniot conditions at the shock:

$$\rho_1 v_1 = \rho_2 v_2, \quad (\text{B1})$$

$$p_1 + \rho_1 v_1^2 = p_2 + \rho_2 v_2^2, \quad (\text{B2})$$

$$\frac{1}{2}v_1^2 + \frac{\gamma p_1}{(\gamma - 1)\rho_1} = \frac{1}{2}v_2^2 + \frac{\gamma p_2}{(\gamma - 1)\rho_2}, \quad (\text{B3})$$

where the subscripts 1 and 2 denote pre- and post-shock quantities. The quantities  $\rho$ ,  $p$ , and  $v$  are the density, pressure, and the velocity of the flow. The stationary mean flow is assumed to be in the positive  $x$  direction and it is characterized by its density  $\bar{\rho}$ , pressure  $\bar{p}$ , and by the  $x$ -components of the velocity  $U$ . The upstream perturbation field consists of entropy and vorticity waves given by equations (2)–(5):

$$\frac{u'_1}{U_1} = l A_v e^{ik(mx + ly - U_1 mt)}, \quad (\text{B4})$$

$$\frac{v'_1}{U_1} = -m A_v e^{ik(mx + ly - U_1 mt)}, \quad (\text{B5})$$

$$\frac{\rho'_1}{\bar{\rho}_1} = A_e e^{ik(mx + ly - U_1 mt)}, \quad (\text{B6})$$

$$\frac{T'_1}{T_1} = -\frac{\rho'}{\bar{\rho}_1}, \quad (\text{B7})$$

where  $m = \cos \psi_1$ ,  $l = \sin \psi_1$ , and  $\psi_1$  is the angle between the  $x$ -axis and the direction of propagation of the incident perturbation.  $u'_1$  and  $v'_1$  are the  $x$ - and  $y$ -components of the velocity fluctuations, while  $A_v$  and  $A_e$  are the amplitudes of the incident vorticity and entropy waves.  $\rho'$  and  $T'$  are the density and temperature perturbations. We ignore the acoustic waves in the upstream field.

When the upstream perturbations hit the shock, the latter responds by changing its position and shape. In the LIA, for a perturbation of form (B4)–(B7), the shock surface deforms into a sinusoidal wave propagating in the  $y$ -direction:

$$\xi(y, t) = -\frac{L}{i\kappa m} e^{i\kappa(l y - U_1 m t)}, \quad (\text{B8})$$

where  $\xi(y, t)$  is the  $x$ -coordinate of the shock position at ordinate  $y$  and time  $t$ .  $L$  is a quantity that characterizes the amplitude of the shock oscillations. The instantaneous velocity  $\xi_t$  and inclination  $\xi_y$  are given by

$$\xi_t(t, y) = U_1 L e^{i\kappa(l y - U_1 m t)}, \quad (\text{B9})$$

$$\xi_y(t, y) = -\frac{l}{m} L e^{i\kappa(l y - U_1 m t)}. \quad (\text{B10})$$

The interaction of the vorticity and entropy waves with the shock generates a downstream perturbation field consisting of vorticity, entropy, and sound waves given by (Mahesh et al. 1996, 1997)

$$\frac{u'_2}{U_1} = F e^{i\kappa x} e^{i\kappa(l y - U_1 m t)} + G e^{i\kappa(C m x + l y - U_1 m t)}, \quad (\text{B11})$$

$$\frac{v'_2}{U_1} = H e^{i\kappa x} e^{i\kappa(l y - U_1 m t)} + I e^{i\kappa(C m x + l y - U_1 m t)}, \quad (\text{B12})$$

$$\frac{p'_2}{\bar{p}_2} = K e^{i\kappa x} e^{i\kappa(l y - U_1 m t)}, \quad (\text{B13})$$

$$\frac{\rho'_2}{\bar{\rho}_1} = \frac{K}{\gamma} e^{i\kappa x} e^{i\kappa(l y - U_1 m t)} + Q e^{i\kappa(C m x + l y - U_1 m t)}, \quad (\text{B14})$$

$$\frac{T'_2}{T_1} = \frac{(\gamma - 1)K}{\gamma} e^{i\kappa x} e^{i\kappa(l y - U_1 m t)} - Q e^{i\kappa(C m x + l y - U_1 m t)}. \quad (\text{B15})$$

The schematic depiction of this process is given in Fig. 1. The coefficients  $F$ ,  $H$ , and  $K$  are the amplitudes of the acoustic component, while coefficients  $G$ ,  $I$ , and  $Q$  are associated with the entropy and vorticity components. The former two components have the same wavenumber vector ( $m\kappa, l\kappa$ ) and angular frequency  $\kappa m U_1$ . The acoustic component has the same angular frequency but different wavenumber ( $\tilde{\kappa}, l\kappa$ ). In order to obtain the latter, we write the wave equation for pressure in the post-shock region (Mahesh et al. 1996):

$$p'_{tt} + 2U_2 p'_{xt} - (c_{s,2}^2 - U_2^2) p'_{xx} - c_s^2 p'_{yy} = 0, \quad (\text{B16})$$

where  $c_{s,2}$  is the speed of sound. The solution in the post-shock region is required to have the same frequency and transverse wavenumber as the incoming perturbation. Thus, the general form of the solution of equation (B16) is

$$p' = F(x) e^{i\kappa(l y - m U_1 t)}. \quad (\text{B17})$$

Assuming  $F(x) \propto e^{\tilde{\kappa} x}$  and substituting this into equation (B16), we obtain a quadratic equation for  $\tilde{\kappa}$ ,

$$\left[ \frac{c_{s,2}^2}{U_1^2} - \frac{U_2^2}{U_1^2} \right] \tilde{\kappa}^2 + 2\kappa m \frac{U_2}{U_1} \tilde{\kappa} - \kappa^2 \left[ m^2 - l^2 \frac{c_{s,2}^2}{U_1^2} \right] = 0. \quad (\text{B18})$$

The discriminant of this equations is real if  $\psi_1 < \psi_c$  and complex if  $\psi_1 > \psi_c$ , where the critical angle  $\psi_c$  is given by equation (13):

$$\psi_c = \cot^{-1} \sqrt{\frac{c_{s,2}^2}{U_1^2} - \frac{U_2^2}{U_1^2}}. \quad (\text{B19})$$

For  $\psi_1 < \psi_c$ ,  $\tilde{\kappa}$  is real and is given by

$$\frac{\tilde{\kappa}}{\kappa} = \frac{U_1}{U_2} \frac{M_2}{1 - M_2^2} \left[ -m M_2 + l \sqrt{\frac{m^2}{l^2} - \frac{U_2^2}{U_1^2} \left( \frac{1}{M_2^2} - 1 \right)} \right]. \quad (\text{B20})$$

In this regime, the solution represents a simple sinusoidal planar sound wave. For  $\psi_1 > \psi_c$ ,  $\tilde{\kappa}$  is complex,  $\tilde{\kappa} = \tilde{\kappa}_r + i\tilde{\kappa}_i$ :

$$\frac{\tilde{\kappa}_r}{\kappa} = -m \frac{U_1}{U_2} \frac{M_2^2}{1 - M_2^2}, \quad (\text{B21})$$

$$\frac{\tilde{\kappa}_i}{\kappa} = l \frac{U_1}{U_2} \frac{M_2}{1 - M_2^2} \sqrt{\frac{U_2^2}{U_1^2} \left( \frac{1}{M_2^2} - 1 \right) - \frac{m^2}{l^2}}. \quad (\text{B22})$$

This describes exponentially damping planar sound wave.

Our next task is to find the amplitudes of the post-shock solution. We start with the linearized Euler equations for the perturbation field (Mahesh et al. 1996):

$$u'_t + U_2 u'_x = -\frac{1}{\bar{\rho}} p'_x, \quad (\text{B23})$$

$$v'_t + U_2 v'_x = -\frac{1}{\bar{\rho}} p'_y. \quad (\text{B24})$$

Substituting the acoustic part of the solutions (7)–(11) into the momentum equation in the  $x$ -direction (B23), we get

$$U_1(-F i \kappa m U_1) + U_2 U_1 F i \tilde{\kappa} = -\frac{1}{\bar{\rho}_2} \bar{p}_2 K i \tilde{\kappa}, \quad (\text{B25})$$

which can be solved for  $F$ ,

$$F = \alpha K, \quad (\text{B26})$$

where we introduced a new variable  $\alpha$  for brevity,

$$\alpha = \frac{c_{s,2}^2}{\gamma U_1^2} \frac{\tilde{\kappa}}{m - \frac{\tilde{\kappa}}{\kappa r}}. \quad (\text{B27})$$

Analogously, the  $y$ -momentum equations yield

$$U_1(-H i \kappa m U_1) + U_2 U_1 H i \tilde{\kappa} = -\frac{1}{\bar{\rho}_2} \bar{p}_2 K i \tilde{\kappa}, \quad (\text{B28})$$

which we solve for  $H$ ,

$$H = \beta K, \quad (\text{B29})$$

where we introduced another variable  $\beta$ ,

$$\beta = \frac{c_{s,2}^2}{\gamma U_1^2} \frac{l}{m - \frac{\tilde{\kappa}}{\kappa r}}. \quad (\text{B30})$$

For vorticity waves, the velocity field has to be solenoidal:

$$U_1 G i \kappa m r + U_1 I i \kappa l = 0, \quad (\text{B31})$$

from which

$$I = -\frac{m r}{l} G. \quad (\text{B32})$$

The Rankine–Hugoniot conditions at the shock yield the following equations for the downstream perturbation field:

$$\frac{u'_2 - \xi_t}{U_1} = B_1 \frac{u'_1 - \xi_t}{U_1} + B_2 \frac{T'_1}{T_1}, \quad (\text{B33})$$

$$\frac{\rho'_2}{\bar{\rho}_2} = C_1 \frac{u'_1 - \xi_t}{U_1} + C_2 \frac{T'_1}{\bar{T}_1}, \quad (\text{B34})$$

$$\frac{p'_2}{\bar{p}_2} = D_1 \frac{u'_1 - \xi_t}{U_1} + D_2 \frac{T'_1}{\bar{T}_1}, \quad (\text{B35})$$

$$\frac{v'_2}{U_1} = \frac{v'_1}{U_1} + E_1 \xi_y, \quad (\text{B36})$$

where  $A, B, C, D, E$  are function of upstream Mach number  $\mathcal{M}_1$  and nuclear dissociating parameter  $\bar{\epsilon}$  only. Substituting the downstream solutions (7)–(11) into these equations, we get a system of algebraic equations for the amplitudes of this solution:

$$F + G - L = B_1(lA_v - L) - B_2A_e, \quad (\text{B37})$$

$$\frac{K}{\gamma} + Q = C_1(lA_v - L) - C_2A_e, \quad (\text{B38})$$

$$K = D_1(lA_v - L) - D_2A_e, \quad (\text{B39})$$

$$H + I = -mA_v - E_1 \frac{l}{m} L. \quad (\text{B40})$$

We normalize the amplitudes of the solutions (7)–(11) with the amplitude of the incident vorticity wave  $A_v$  (i.e.  $\tilde{F} = F/A_v$ ,  $\tilde{L} = L/A_v$ , etc.). We rewrite the above system using these coefficients:

$$\tilde{F} = \alpha \tilde{K}, \quad (\text{B41})$$

$$\tilde{H} = \beta \tilde{K}, \quad (\text{B42})$$

$$\tilde{I} = -\frac{mr}{l} \tilde{G}, \quad (\text{B43})$$

$$\tilde{F} + \tilde{G} - \tilde{L} = B_1(l - \tilde{L}) - B_2 \frac{A_e}{A_v}, \quad (\text{B44})$$

$$\frac{\tilde{K}}{\gamma} + \tilde{Q} = C_1(l - \tilde{L}) - C_2 \frac{A_e}{A_v}, \quad (\text{B45})$$

$$\tilde{K} = D_1(l - \tilde{L}) - D_2 \frac{A_e}{A_v}, \quad (\text{B46})$$

$$\tilde{H} + \tilde{I} = -m - E_1 \frac{l}{m} \tilde{L}. \quad (\text{B47})$$

The solution of this system is

$$\tilde{L} = \frac{-m - \beta \left( D_1 l - D_2 \frac{A_e}{A_v} \right)}{E_1 \frac{l}{m} - \beta D_1 - \frac{mr}{l} (1 - B_1 + \alpha D_1)} + \frac{\frac{mr}{l} \left[ -\alpha \left( D_1 l - D_2 \frac{A_e}{A_v} \right) + B_1 l - B_2 \frac{A_e}{A_v} \right]}{E_1 \frac{l}{m} - \beta D_1 - \frac{mr}{l} (1 - B_1 + \alpha D_1)}, \quad (\text{B48})$$

$$\tilde{I} = -\frac{mr}{l} \left[ (1 - B_1 + \alpha D_1) \tilde{L} - \alpha \left( D_1 l - D_2 \frac{A_e}{A_v} \right) + B_1 l - B_2 \frac{A_e}{A_v} \right], \quad (\text{B49})$$

$$\tilde{G} = \tilde{L} (1 - B_1 + \alpha D_1) - \alpha \left( D_1 l - D_2 \frac{A_e}{A_v} \right) + B_1 l - B_2 \frac{A_e}{A_v}, \quad (\text{B50})$$

$$\tilde{K} = D_1(l - \tilde{L}) - D_2 \frac{A_e}{A_v}, \quad (\text{B51})$$

$$\tilde{F} = \alpha D_1(l - \tilde{L}) - \alpha D_2 \frac{A_e}{A_v}, \quad (\text{B52})$$

$$\tilde{H} = \beta \left( D_1 l - D_2 \frac{A_e}{A_v} \right) - \beta D_1 \tilde{L}, \quad (\text{B53})$$

$$\tilde{Q} = C_1(l - \tilde{L}) - C_2 \frac{A_e}{A_v} - \frac{D_1}{\gamma} (l - \tilde{L}) + \frac{D_2}{\gamma} \frac{A_e}{A_v}. \quad (\text{B54})$$

We find that the solution depends on the upstream Mach number  $\mathcal{M}_1$  of the mean flow, the nuclear dissociation parameter  $\bar{\epsilon}$ , and the ratio of the amplitudes of the upstream entropy and vorticity waves  $A_e/A_v$ . Note that none of the amplitude functions depends on the wavenumber  $\kappa$  of the incident waves, so the LIA solution is invariant with respect to the spatial scale of the incoming perturbations.

This paper has been typeset from a  $\text{\LaTeX}$  file prepared by the author.